Research Article

Nonisolated DC to DC Converters for High-Voltage Gain Applications Using the MPPT Approach

C. Subba Rami Reddy ⓘ,[1] **Bharath Kumar Narukullapati** ⓘ,[2] **M. Uma Maheswara Rao** ⓘ,[2] **Sangu Ravindra** ⓘ,[3] **P. M. Venkatesh** ⓘ,[2] **T. Ch. Anil Kumar** ⓘ,[4] **B. Mouli Chandra** ⓘ,[5] **and Afework Aemro Berhanu** ⓘ[6]

[1]*Department of Electrical and Electronics Engineering, B. V. Raju Institute of Technology, Vishnupur 502313, India*
[2]*Department of Electrical and Electronics Engineering, Vignan's Foundation for Science Technology and Research, Guntur 522213, India*
[3]*Department of Electrical and Electronics Engineering, VVIT, Nambur, Guntur, Andhra Pradesh, India*
[4]*Department of Mechanical Engineering, Vignan's Foundation for Science Technology and Research, Guntur 522213, India*
[5]*Department of Electrical and Electronics Engineering, QIS College of Engineering & Technology, Ongole 523272, India*
[6]*Department of Environmental Engineering, College of Biological and Chemical Engineering, Addis Ababa Science and Technology University, Addis Ababa, Ethiopia*

Correspondence should be addressed to Afework Aemro Berhanu; afework.aemro@aastu.edu.et

It is proved and examined in this research paper that the perturb and observe (P and O) technique for isolating the photovoltaic array (PVA) from the power structure may be used to isolate the PV array from the power structure. A single specified voltage setup can remove the maximum power from a PV cell because of the nonlinear properties of the PV cell's output. As a result, in PVA, the maximum power point tracking (MPPT) algorithm is utilized to increase the yield control range by increasing the maximum power point. In this study, the MPPT computations are carried out with the assistance of a DC-DC boost converter for usage in applications needing high voltage gain at a variety of sun-positioned irradiances and cell temperatures, as demonstrated in the literature.

1. Introduction

The incorporation of renewable energy sources such as solar photovoltaics and fuel cells has increased the popularity of DC microgrids [1]. Beyond their original use in renewable energy conversion, high-gain dc-dc converters have found widespread adoption in a variety of other fields, including battery backup systems for uninterrupted power supplies, and high-intensity discharge lamp ballasts for automobile headlamps, electric tractions, and even some medical equipment [2–4]. Since high-frequency transformers may be configured to support any required turns ratio, isolated DC-DC converters and coupled inductor type converters using these devices can deliver significant voltage gain [5]. Electricity generated from renewable sources can be used to

power outlying locations when combined with the grid. Increased availability of grid-connected PV systems can be attributed to the development of DC-DC converter topologies and inverter control methods. Power feed efficiency is highly dependent on the DC-DC converter stage being properly selected and operating at peak efficiency [6]. When connecting the dc microgrid, high-efficiency high-gain DC-DC converters are required because of the low output voltage of these dc power generators. When it comes to photovoltaics, it is best known as a process for generating electric power by converting solar-generated energy into electrical energy through the photovoltaic effect [7]. PV cells generate direct current as the electrical source from light, which can be used to power DC equipment or to recharge a battery, depending on their orientation [8]. Initially,

photovoltaics were used to control satellites and other rockets in the vicinity; however, today, the vast majority of photovoltaic modules [9, 10] are used for cross-sectional related applications with the assistance of power electronic converters and to generate enormous amounts of energy, which was the original rationale for their use. The typical yield of a PV module is determined by the daylight-based irradiance and the air temperature, and the yield voltage of a PV module is determined by the relationship between PV modules. It is critical to demonstrate and reauthorize for maximum power point tracking (MPPT) [11] of PV array applications because PV modules have nonlinear characteristics, and the yield is dependent on solar radiation [12]. Various MPPT procedures have been used in the past, but the bother and watch (P&O) calculation is the most widely recognized and ideal for use by industry because of its straightforwardness and ease of execution [13]. As a result, this calculation continues to be the most widely used [14].

In order to make use of the P&O calculation, the controller changes voltage if the deliberate power is more prominent or less prominent than the previous estimation of intensity [15]. The controller makes alterations in a similar manner until there is no greater increment or decrement in power [16]. Figure 1 depicts the block diagram of a PVA structure that makes use of a boost converter [17].

2. PV Panel

An electronic device that converts solar power into electrical power is known as a photovoltaic cell. The power rating of a solar-powered [18] board is determined by the size of the PV board and the arrangement of modules within the board; as a result, the voltage rating and current evaluations change, while the power rating remains constant. Because a single PV panel may not be able to generate the necessary amount of power, we connect multiple panels in series or parallel to meet our needs. Series association of PV board increment voltage rating in a series arrangement and parallel association of PV board increment current rating in a parallel arrangement is done [19]. The electrical equivalent of the PV panel is shown in Figure 2.

The I-V characteristics of the PV module are depicted in Figure 3 at a cell temperature of 25°C. A PV cell's output current can be determined by applying KCL and given in the following equation:

$$I_{pv} = I_{scc} - I_D - I_{sh}, \tag{1}$$

where I_{pv} = PV module current, I_{scc} = photo current (or) solar cell current, I_D = diode current, and I_{sh} = shunt current.

The current-voltage attributes condition of a PV module is depicted as given in the following equation:

$$I_{pv} = N_p I_{ph} - I_{rs} \left(e^{\left(\left(q \left(V_{pv} + \left(R_s I_{pv} \right) \right) \right) / \left(N_s \text{AKT} \right) \right)} - 1 \right)$$
$$- \frac{V_{pv} + I_{pv} R_{rs}}{R_{sh}}, \tag{2}$$

where q = electron charge ($1.602 * 10^{-19}$C), N_s = number of sun-based cells related in plan in series, N_p = number of

daylight-based cells related in parallel, I_{rs} = reverse saturation current, T = total temperature, K = Boltzmann constant ($1.38 * 10^{-23}$ J/K).

Also,

$$I_{ph} = I_{sc} + \frac{K_i (T - 298) G}{100},$$
$$I_0 = I_{rs} \left[\frac{T}{T_r} \right]^3 \left(e^{\left((q e g_0) / (N_s \text{AKT}) \right) \left[(1/T_r) - (1/T) \right]} \right), \tag{3}$$

where I_{sc} = short out current of PV module at standard test states of 25°C and 1000 W/m², K_i = temperature coefficient of short out current, G = the sun-based lights. The turnaround immersion current of the PV module is given in the following equation:

$$I_{rs} = \frac{I_{sc}}{\left(e^{\left((q V_{oc}) / (n N_s \text{KT}) \right)} - 1 \right)}, \tag{4}$$

where n = the dreamer factor of the diode = 1.3 V_{oc} = open circuit voltage. The current through the shunt resistor of the above PV module is given in the following equation:

$$I_{sh} = \frac{V_{pv} + I_{pv} R_{rs}}{R_{sh}}. \tag{5}$$

The most common photovoltaic system applications are on rooftops and in buildings, and they include concentrator photovoltaic systems, photovoltaic thermal hybrid solar collectors, rural electrification systems, standalone systems, spacecraft applications, specialty power systems, and specialty lighting systems [20].

3. DC-DC Boost Converter

The boost converter is a converter that has an output voltage that is higher than the source voltage. Boost converters are used in data conversion [21]. It is additionally referred to as a step-up converter. Whenever the feedback regulation is functioning properly, the control loop keeps the output voltage where it needs to be, and the converter operates at a duty cycle below the critical level [22]. However, when the feedback loop is saturated by excessive load current, inadequate input power [23], or an increase in the resistance of the converter switches, the output voltage drops below the desired value [24]. When the controller's duty cycle goes above a certain threshold, the conversion gain goes negative [25]. The gain polarity inversion and excessive inductor current can be prevented by fixing the duty-cycle limit [26].

A regular DC-DC converter circuit is depicted in Figure 4.

It is a switching converter that operates by intermittently opening and closing a power electronic switch, as described above. DC voltage source, inductor L, controlled semiconductor switch (S), diode (D), capacitor (C), and load containment (R) are the components of the boost converter. MOSFETs, IGBTs, and BJTs are the semiconductor switches
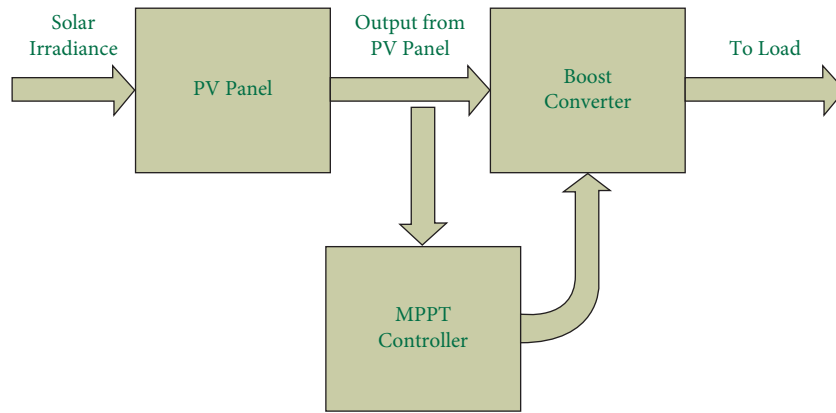
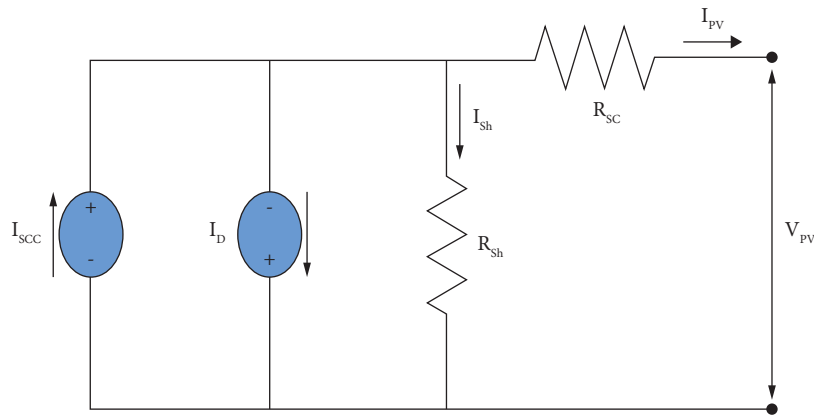FIGURE 1: Block diagram of the boost converter with the MPPT controller.

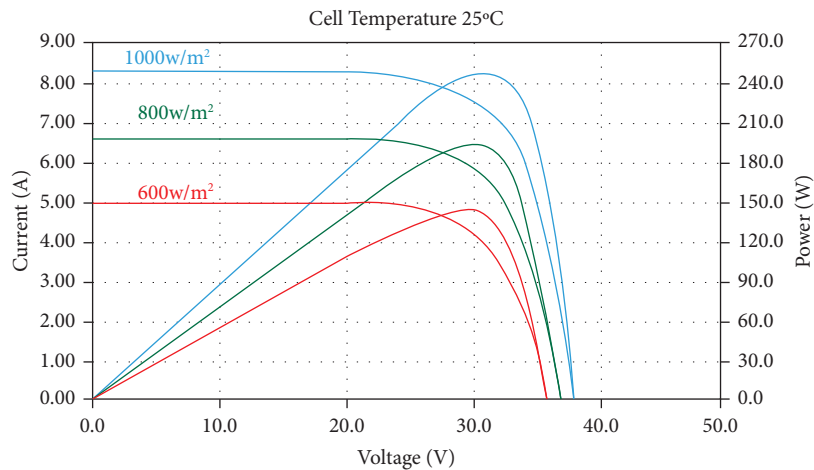FIGURE 2: The electrical equivalent of the PV panel.

FIGURE 3: I-V and P-V characteristics of the PV module.

that are used in this converter. MOSFET is utilized due to the fact that it is a voltage-controlled device, and its switching frequency is higher. It also requires little current, which has a high switching rate and operates in the mill amperes per second range. There are two modes of operation available in this converter.

3.1. Methods of Activity

3.1.1. Mode-1. When switch S is turned off, diode D is turned unevenly, to be precise. The inductor is connected in series with the source and charges up, causing the inductor current to expand. Because of the inductor's high voltage, it
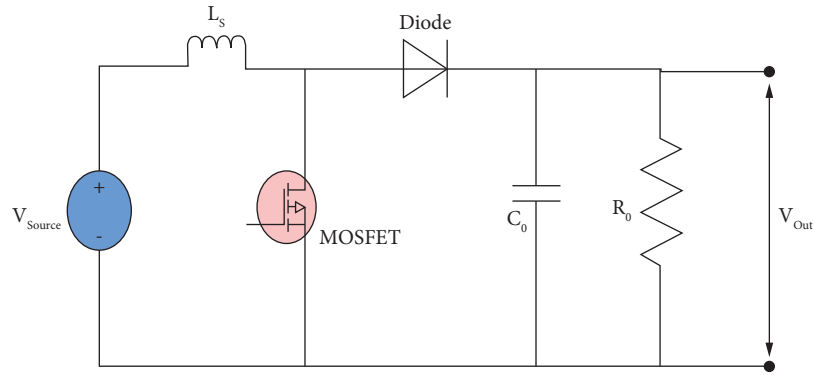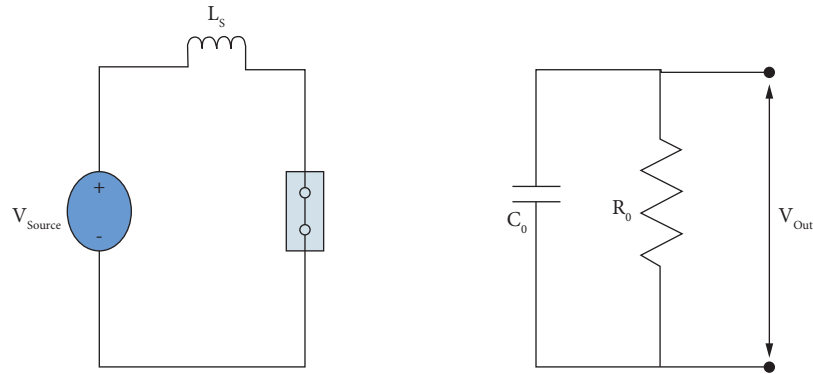
FIGURE 4: Conventional DC-DC boost converter.

FIGURE 5: Conventional DC-DC boost converter in ON-state (switch shunt).

is comparable to the data voltage. The on-state circuit diagram of the converter is shown in Figure 5.

$$V_{\text{source}} = L \frac{di_L}{dt},$$

$$\Delta i_{L_{\text{opened}}} = \frac{DTV_{\text{source}}}{L}. \tag{6}$$

3.1.2. Mode-2. As soon as switch S is activated, diode D is in the forward uneven state. The current flows towards the stack, causing the regard to escape the inductor's and information's centrality in the circuit. The circuit diagram of a typical DC-DC support converter is shown in Figure 6 when the turn is opened in the OFF state.

$$V_L = V_{\text{source}} - V_{\text{out}},$$

$$\Delta i_{L_{\text{closed}}} = (V_{\text{source}} - V_{\text{out}}) \frac{(1-D)T}{L}, \tag{7}$$

$$V_{\text{source}} - V_{\text{out}} = L \frac{di_L}{dt}.$$

In steady-state operation,

$$\Delta i_{L_{\text{opened}}} + \Delta i_{L_{\text{closed}}} = 0. \tag{8}$$

The yield voltage condition of the lift converter is

$$V_{\text{source}} T_{\text{ON}} + (V_{\text{source}} - V_{\text{out}}) T_{\text{OFF}} = 0,$$

$$V_{\text{source}} T_{\text{ON}} + V_{\text{source}} T_{\text{OFF}} = V_{\text{out}} T_{\text{OFF}},$$

$$V_{\text{source}} (T_{\text{ON}} + T_{\text{OFF}}) = V_{\text{out}} T_{\text{OFF}},$$

$$\frac{V_{\text{out}}}{V_{\text{source}}} = \frac{T_{\text{ON}} + T_{\text{OFF}}}{T_{\text{OFF}}} \tag{9}$$

$$= \frac{T_S}{T_{\text{OFF}}} = \frac{1}{(1-D)}.$$

The output current equation of the boost converter can be deduced from the equation shown in Figure 7. During the off-time, it provides the output circuit. During on-time, the inductor-free wheels on the source side result in no current being delivered to the load during on-time.

$$V_{\text{source}} T_{\text{OFF}} = V_{\text{out}} T_s,$$

$$\frac{T_S}{T_{\text{OFF}}} = \frac{1}{(1-D)},$$

$$V_{\text{out}} = V_{\text{source}} (1 - D), \tag{10}$$

$$V_{\text{source}} T_s = V_{\text{out}} T_0,$$

$$V_{\text{source}} I_L = \frac{[(V_{\text{source}}/(1-D))]^2}{R}.$$
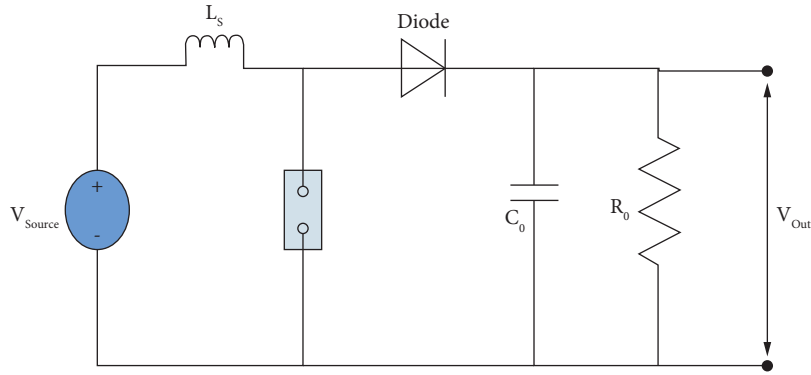
FIGURE 6: Conventional DC-DC boost converter in OFF-state (switch opened).

FIGURE 7: Flow chart of perturbation and observation.

From the above condition, we can discover normal inductor current as given in the following equation:

$$I_L = \frac{V_{\text{source}}}{R(1-D)^2}. \tag{11}$$

The most extreme inductor current can be composed as given in the following equation:

$$I_{L\max} = I_L - \frac{\Delta I_L}{2} = \frac{V_{\text{source}}}{R(1-D)^2} - \frac{V_{\text{source}}}{\text{DT}2L}. \tag{12}$$

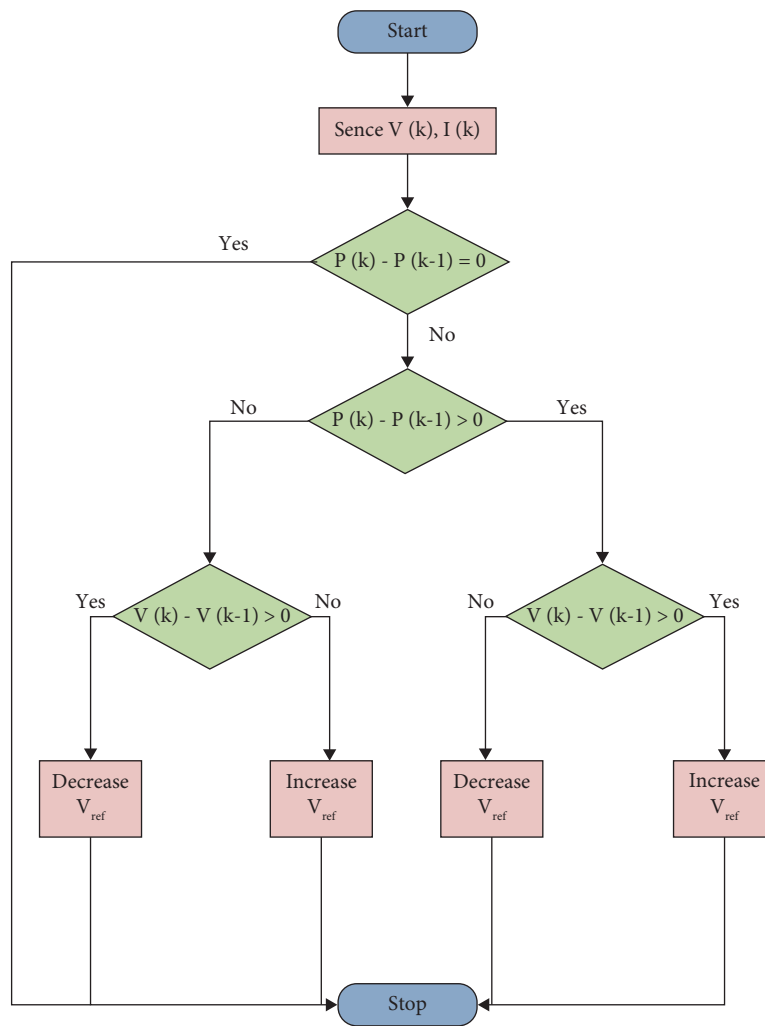The base estimation of the inductance and the base estimation of the capacitor for the predictable current mode can be formed using the equations given in the previous section equation.

$$I_{L\min} \geq 0,$$

$$L_{\min} = \frac{D(1-D)^2 R}{2}. \tag{13}$$

The swell factor and the base estimation of capacitor for nonstop current mode can be formed as shown in the following equation:

$$\Delta Q = \frac{V_{\text{out}} DT}{R} = C\Delta V_{\text{out}}, \tag{14}$$

$$\Delta V_{\text{out}} = \frac{V_{\text{out}} DT}{RC} = \frac{V_{\text{out}} D}{RCf}, \tag{15}$$

$$r = \frac{\Delta V_{\text{out}}}{V_{\text{out}}}, \tag{16}$$

$$C_{\min} = \frac{V_{\text{out}} D}{\Delta V_{\text{out}} Rf}. \tag{17}$$

4. MPPT Controller

Estimates of MPPT (maximum power point tracking) are integrated into a charge controller and used for evacuating the majority of extraordinary open power structure PV modules under explicit conditions. This maximum power point tracking technique adjusts the boost converter duty cycle step size based on the input conditions of the system. This procedure begins by calculating the differential value of the instantaneous radiation, photovoltaic voltage and current, and load power. This technique maximises the duty cycle during constant radiation conditions, allowing the MPPT algorithm to track more quickly [27]. There is a transitory period of oscillations with the irradiance change. Because of these extraneous variations in weather, it is necessary that everything gradually converges on the MPP. The voltage at which a PV module can produce the maximum amount of power is referred to as the maximum power point. MPPT (maximum power point tracking) is a technique used in PV board charge controllers to track the maximum power point, known as a maximum power point technique (MPPT), and an electronic DC-DC converter is a device that improves the match between a solar-powered showcase (PV sheets) and a battery bank or a power-generation structure. No, the MPPT is not a mechanical after structure that physically moves the modules in order to make their point even more authentical at the sun [28]. MPPT is a completely electronic/modernized system that is responsible for the electrical operation of the module. The majority of today's MPPT charge controllers are approximately 93–95 percent effective in the transformation; however, the very best MPPT charge controllers can be up to 97–99 percent effective. Duty-cycle control works by

comparing the power output of a PV module (determined by multiplying its voltage by its current) to its output from a prior cycle. The duty is controlled so that the maximum power point is maintained, and this is determined by comparing the current sample value of the voltage to the prior value in the same manner as before. To determine the optimal power point tracking methodology, the duty cycle is compared to the power and voltage [29].

P&O calculation, gradual conductance, and other calculations are performed by the MPPT controller [30]. The first of these calculations is performed by the P&O calculation.

In order to make use of the correlation between PV module voltage and power output, the P&O technique is employed. By adjusting the voltage in the direction of increasing the power, the maximum power point can be tracked by observing the resulting change in power. In order to determine the link between the power output and the voltage input of a solar cell, the incremental conductance method makes use of the slope of the power-voltage (P-V) curve. Maximum power is reached at a voltage of zero, with the voltage increasing when the slope is positive and decreasing when the slope is negative [31].

Within the scope of this work, we presented how the P&O method can be utilised. Because of its simplicity and ease of implementation, the perturb and observe (P&O) approach is extensively employed as an MPPT algorithm for PV system applications [32]. The method introduces disturbances to the duty cycle by either increasing or reducing it by a constant duty step size and then monitors the effects on the PV system's output power [33]. If the change in output power is more than zero, the operating point has shifted closer to the maximum power point (MPP) [34], and the duty cycle will continue to be perturbed in the same direction [35]. The cycle will continue until the maximum physiological state (MPS) is reached and maintained [36]. Unfortunately, the steady-state operating point of this algorithm oscillates about the MPP. This causes a minor drop in PV efficiency. Reducing the duty cycle dampens the steady-state oscillation but slows down the dynamic response. Therefore, the duty cycle must be properly adjusted to achieve a balance between the two [37]. The P&O calculation graph is illustrated in Figure 7.

4.1. Drawbacks

(1) If the voltage is far away from the MPP, the P&O technique is only moderately effective in locating the MPP [29]

(2) Small (and fixed) gradual changes are used in the P&O strategy to produce a large transient following time "t" is defined as the amount of time it takes an MPPT calculation to reach within 95 percent of the most extreme normal power available at MPP

5. Simulation Results

The simulation diagram of a PV board is shown in Figures 8 and 9. The I-V traits and P-V attributes of the PV board are plotted and shown in Figures 10 and 11, respectively.
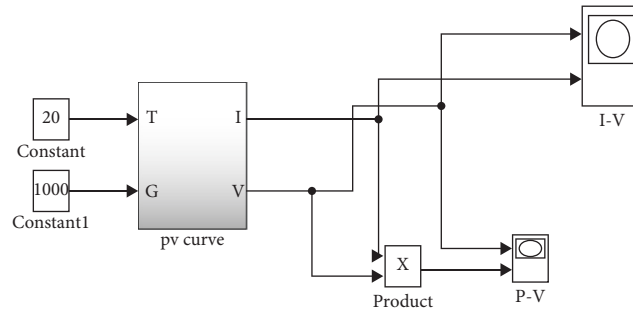
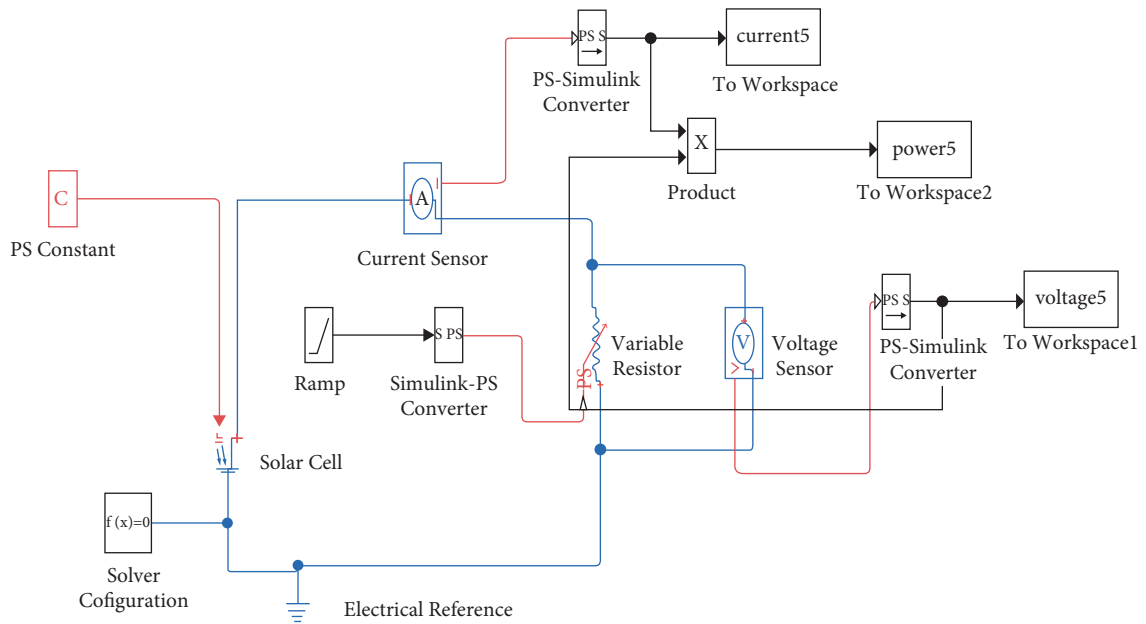Figure 8: Simulation diagram of the PV board.

Figure 9: Schematic representation of a simulation used to determine solar cell characteristics.
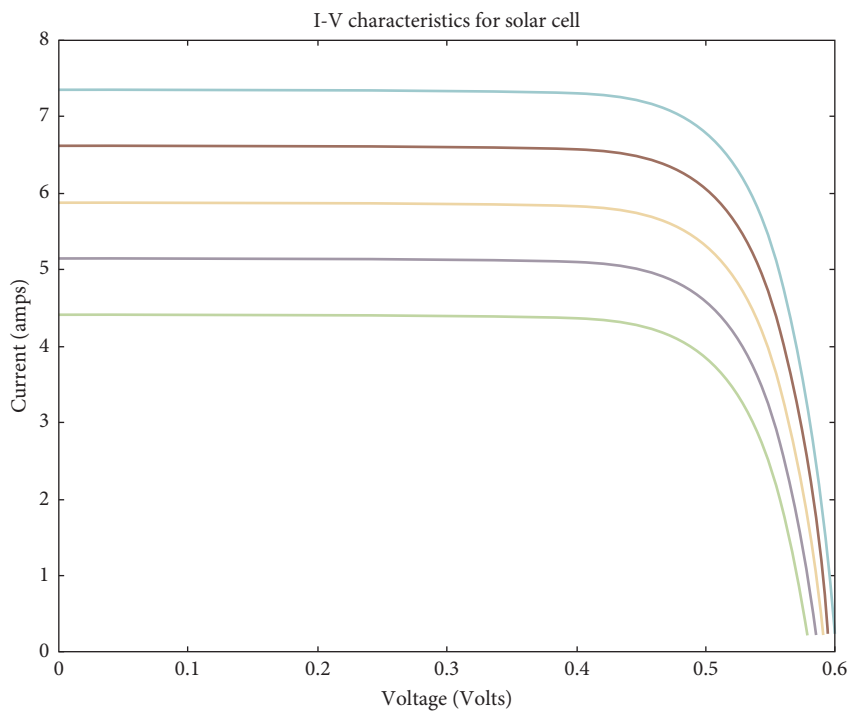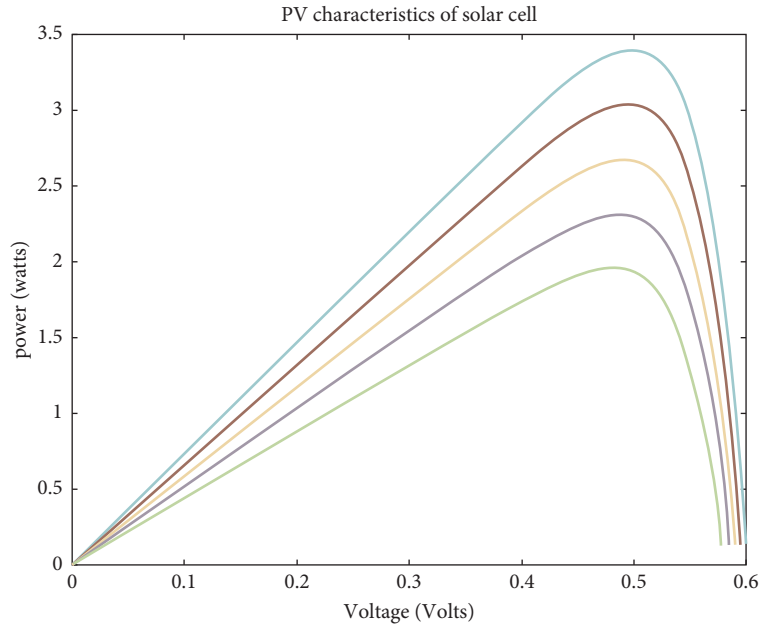

Figure 10: I-V traits of the PV board.

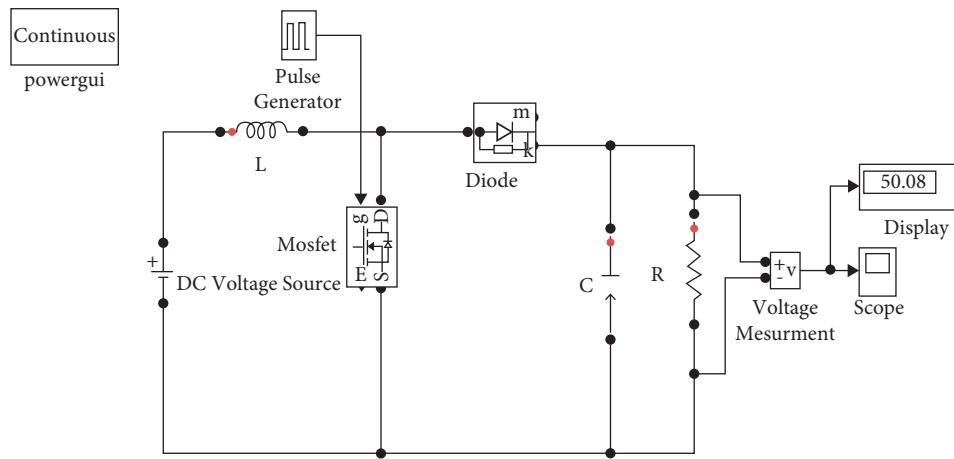FIGURE 11: P-V attributes of the PV board.

FIGURE 12: Simulation diagram of the typical boost converter.

FIGURE 13: After-effect of the boost converter.
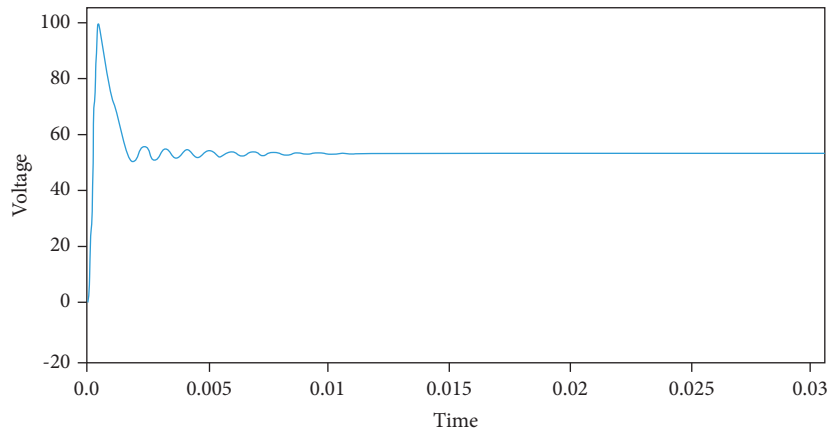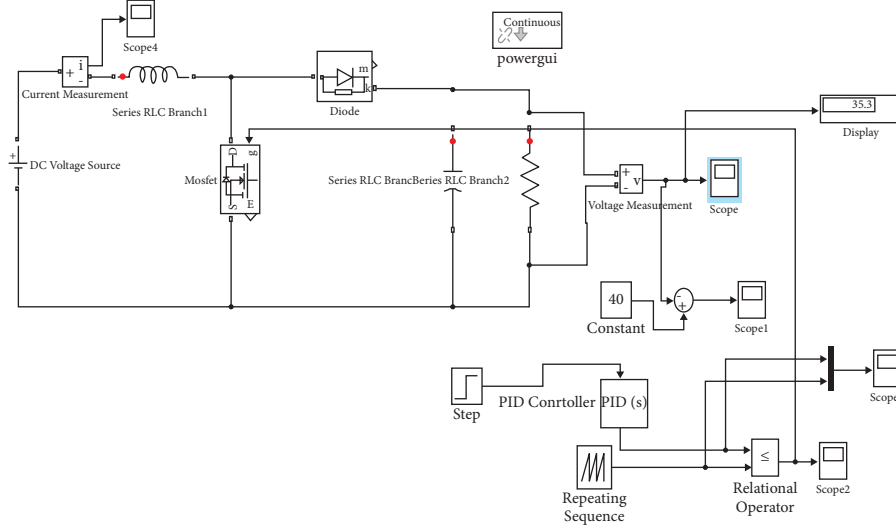
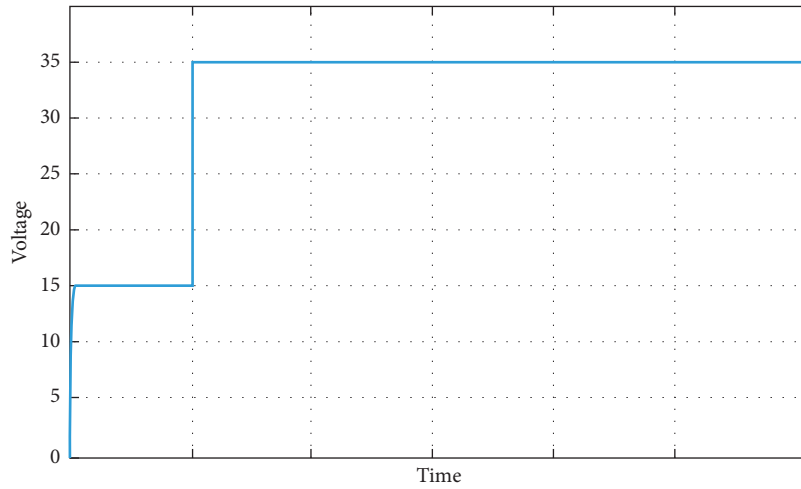FIGURE 14: Simulation diagram of the boost converter.

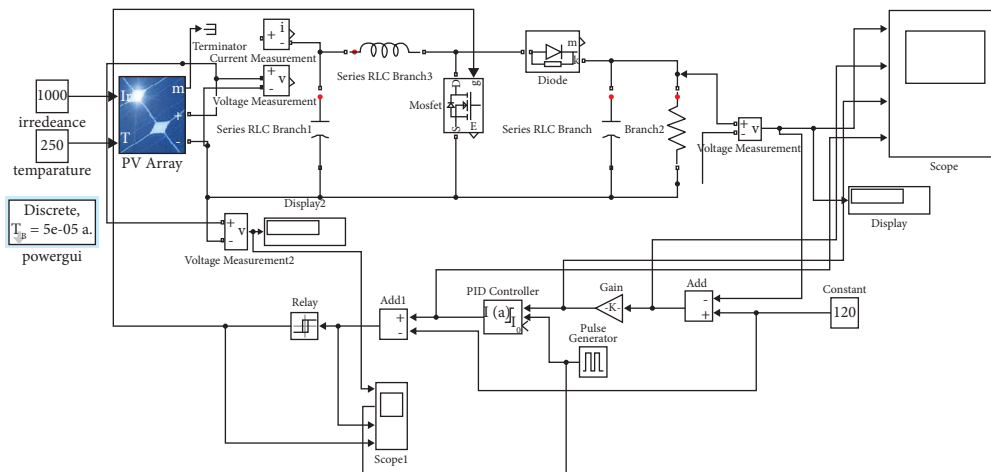FIGURE 15: Converter voltage waveform.

FIGURE 16: Simulation diagram of PV with the boost converter.
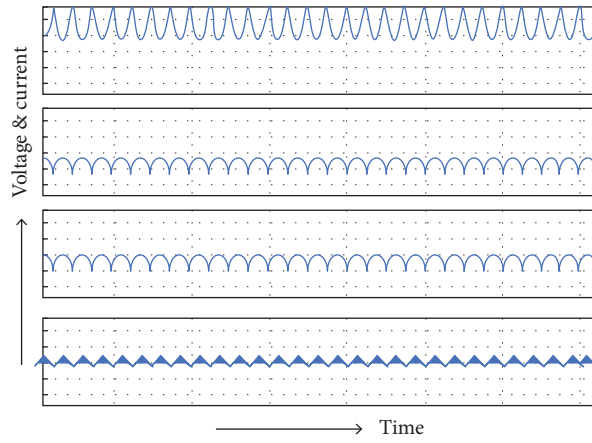
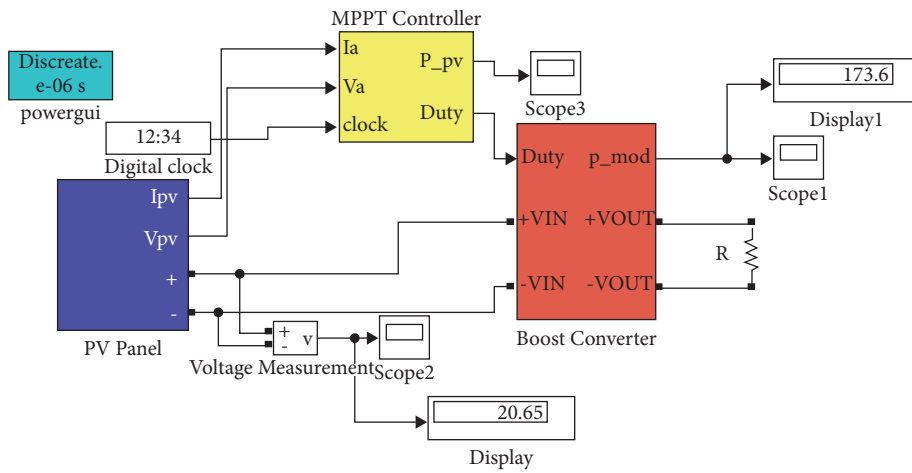FIGURE 17: Output voltage and current waveforms of PV with the boost converter.

FIGURE 18: Simulation diagram of solar MPPT with the boost converter.
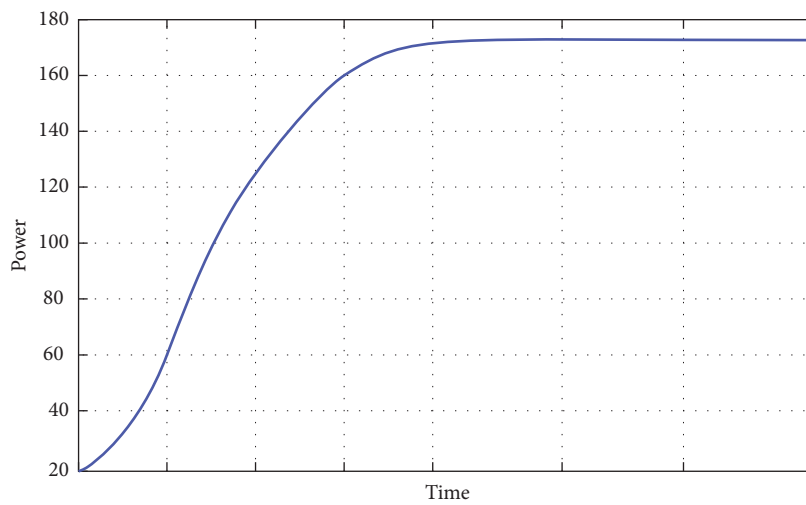

FIGURE 19: Power curve of solar MPPT with the boost converter.

The simulation diagrams of the boost converter are shown in Figures 12 and 13. The voltage waveform of the after-effect of the boost converter and converter voltage waveform are shown in Figures 14 and 15, respectively.

The simulation diagram of the PV module with the boost converter is designed and illustrated in Figure 16, and the associated output voltage and current waveforms of PV with the boost converter are shown in Figure 17.

The simulation diagram of solar MPPT with boost converter is designed and illustrated in Figure 18, and the power waveform of solar MPPT with boost converter is shown in Figure 18. Power curve of solar MPPT with boost converter is shown in Figure 19.

6. Conclusion and Future Works

In this article, the P&O algorithm is used to track the maximum power point and is given as input to the DC-DC converters which are operating at a high duty cycle ratio. The converter considered here will function properly at a high duty cycle to prevent the excessive inductor current. Due to the ease with which it can be implemented and due to its top-level viability, the perturb and observe MPPT system is used in our methodology. As an alternative, a modified P&O MPPT algorithm can be designed to stabilize the output voltage under rapid radiation change conditions and varied load conditions in our future works, which is especially useful for small or domestic PV systems.

Data Availability

The data used to support the findings of this study are included within the article. Should further data or information be required, these are available from the corresponding author upon request.

Conflicts of Interest

The authors declare that there are no conflicts of interest regarding the publication of this paper.

Acknowledgments

References

[1] M. Lakshmi and S. Hemamalini, "Nonisolated high gain DC-DC converter for DC microgrids," *IEEE Transactions on Industrial Electronics*, vol. 65, no. 2, pp. 1205–1212, 2018.

[2] B. Bryant and M. K. Kazimierczuk, "Voltage-loop power-stage transfer functions with MOSFET delay for boost PWM converter operating in CCM," *IEEE Transactions on Industrial Electronics*, vol. 54, no. 1, pp. 347–353, 2007.

[3] X. Wu, J. Zhang, X. Ye, and Z. Qian, "Analysis and derivations for a family ZVS converter based on a new active clamp ZVS cell," *IEEE Transactions on Industrial Electronics*, vol. 55, no. 2, pp. 773–781, 2008.

[4] F. L. Tofoli, D. D. C. Pereira, W. Josias de Paula, and D. D. S. Oliveira Júnior, "Survey on non-isolated high-voltage step-up dc-dc topologies based on the boost converter," *IET Power Electronics*, vol. 8, no. 10, pp. 2044–2057, 2015.

[5] M.-K. Nguyen, T.-D. Duong, Y.-C. Lim, and Y.-J. Kim, "Isolated boost DC-DC converter with three switches," *IEEE Transactions on Power Electronics*, vol. 33, no. 2, pp. 1389–1398, 2018.

[6] B. Sri Revathi and M. Prabhakar, "Non isolated high gain DC-DC converter topologies for PV applications - a comprehensive review," *Renewable and Sustainable Energy Reviews*, vol. 66, pp. 920–933, 2016.

[7] H. F. Abdul Wahab and H. Sanusi, "Simulink Model of Direct torque control of induction machine," *American Journal of Applied Sciences*, vol. 5, no. 8, pp. 1083–1090, 2008.

[8] C. L. Toh, N. R. N. Idris, and A. H. M. Yatim, "Torque ripple reduction in direct torque control of induction motor drives," power engineering conference," Bangi, Malaysia, December 2003.

[9] Y. Hayashi, Y. Matsugaki, and T. Ninomiya, "Design consideration for high step-up nonisolated multicellular dc-dc converter for PV micro converters," *Journal of Engineering*, vol. 2018, Article ID 5098083, 16 pages, 2018.

[10] K. Mohan Reddy and A. Naveen Reddy, "Solar PV array fed four switch buck-boost converter for LHB coach," *International Journal of Control Theorey and Applications*, vol. 9, no. 29, pp. 249–255, 2016.

[11] A. Naveen Reddy, "Performance and improvement of induction motor by using multilevel," *Inverter" International Journal of Control Theorey and Applications*, vol. 9, no. 10, pp. 4211–4219, 2016.

[12] P. V. S. Sobhan, M. Subba Rao, N. Bharath Kumar, and A. Sriharibabu, "Design of fuzzy logic based photovoltaic fed battery charging system," *Journal of Green Engineering (JGE)*, vol. 9, no. 2, pp. 270–281, 2019.

[13] F. M. Shahir and E. Babaei, "Application of high voltage gain DC-DC converter in photovoltaic system with energy storage," in *Proceedings of the 2017 8th Power Electronics, Drive Systems & Technologies Conference (PEDSTC)*, pp. 265–269, IEEE, Mashhad, Iran, Feburary 2017.

[14] H. Shayeghi, S. Pourjafar, S. Majid Hashemzadeh, and F. Sedaghati, "Presenting of the magnetic coupling-based transformer-less high step-up DC-DC converter for renewable energy applications," *International Transactions on Electrical Energy Systems*, vol. 2022, Article ID 3141119, 15 pages, 2022.

[15] V. R. Teja, S. Srinivas, and M. K. Mishra, "A three port high gain non-isolated DC-DC converter for photovoltaic applications," in *Proceedings of the 2016 IEEE International Conference on Industrial Technology (ICIT)*, pp. 251–256, IEEE, Taipei, Taiwan, March 2016.

[16] M. H. Taghvaee, M. A. M. Radzi, S. M. Moosavain, H. Hizam, and M. Hamiruce Marhaban, "A current and future study on non-isolated DC-DC converters for photovoltaic applications," *Renewable and Sustainable Energy Reviews*, vol. 17, pp. 216–227, 2013.

[17] C. Balakishan, N. Sandeep, and M. V. Aware, "Design and implementation of three-level DC-DC converter with golden section search based MPPT for the photovoltaic applications," *Advances in Power Electronics*, vol. 2015, Article ID 587197, 9 pages, 2015.

[18] S. Thangavelu and P. Umapathy, "Design of new high step-up DC-DC converter topology for solar PV applications,"

International Journal of Photoenergy, vol. 2021, Article ID 7833628, 11 pages, 2021.

[19] P. K. Maroti, S. Padmanaban, F. Blaabjerg, L. Martirano, and P. Siano, "A novel multilevel high gain modified SEPIC DC-to-DC converter for high voltage/low current renewable energy applications," in *Proceedings of the 2018 IEEE 12th International Conference on Compatibility, Power Electronics and Power Engineering (CPE-POWERENG 2018)*, pp. 1–6, IEEE, Doha, Qatar, April 2018.

[20] C. Muranda, E. Ozsoy, S. Padmanaban, M. S. Bhaskar, V. Fedák, and V. K. Ramachandaramurthy, "Modified SEPIC DC-to-DC boost converter with high output-gain configuration for renewable applications," in *Proceedings of the 2017 IEEE Conference on Energy Conversion (CENCON)*, pp. 317–322, IEEE, Kuala Lumpur, Malaysia, October 2017.

[21] K. Nagarajan, A. Rajagopalan, S. Angalaeswari, L. Natrayan, and W. D. Mammo, "Combined economic emission dispatch of microgrid with the incorporation of renewable energy sources using improved mayfly optimization algorithm," *Computational Intelligence and Neuroscience*, vol. 2022, Article ID 6461690, 22 pages, 2022.

[22] S. Mahapatra, S. S. Parida, K. Surana, P. Balamurugan, L. Natrayan, and P. Paramasivam, "Energy auditing for efficient planning and implementation in commercial and residential buildings," *Advances in Civil Engineering*, vol. 2021, Article ID 1908568, 10 pages, 2021.

[23] G. Kanimozhi, L. Natrayan, S. Angalaeswari, and P. Paramasivam, "An effective charger for plug-in hybrid electric vehicles (PHEV) with an enhanced PFC rectifier and ZVS-ZCS DC/DC high-frequency converter," *Journal of Advanced Transportation*, vol. 2022, Article ID 7840102, 14 pages, 2022.

[24] L. Natrayan, P. S. S. Sundaram, and J. Elumalai, "Analyzing the Uterine physiological with MMG Signals using SVM," *International journal of pharmaceutical research*, vol. 11, no. 2, pp. 165–170, 2019.

[25] S. S. Sundaram, N. H. Basker, and L. Natrayan, "Smart clothes with bio-sensors for ECG monitoring," *International Journal of Innovative Technology and Exploring Engineering*, vol. 8, no. 4, pp. 298–301, 2019.

[26] V. Michal, "Dynamic duty-cycle limitation of the boost DC/DC converter allowing maximal output power operations," in *Proceedings of the 2016 International Conference on Applied Electronics (AE)*, pp. 177–182, IEEE, Pilsen, Czech Republic, September 2016.

[27] K. Javed, H. Ashfaq, and R. Singh, "An improved MPPT algorithm to minimize transient and steady state oscillation conditions for small SPV systems," *International Journal of Renewable Energy Development*, vol. 7, no. 3, pp. 191–197, 2018.

[28] A. Abusorrah and M. M. Al-Hindawi, Y. Al-Turki, K. Mandal, D. Giaouris, S. Banerjee, S. Voutetakis, S. Papadopoulou, Stability of a boost converter fed from photovoltaic source," *Solar Energy*, vol. 98, pp. 458–471, 2013.

[29] E. Ozsoy, S. Padmanaban, V. Fedak, C. Muranda, and M. Cernet, "Modified SEPIC DC-to-DC converter 2/(1-k) output gain configuration for renewable power energy and high voltage applications," in *Proceedings of the 2018 IEEE 18th International Power Electronics and Motion Control Conference (PEMC)*, pp. 145–149, IEEE, Budapest, Hungary, August 2018.

[30] P. Sanjeevikumar, G. Grandi, P. W. Wheeler, F. Blaabjerg, and J. Loncarski, "A simple MPPT algorithm for novel PV power generation system by high output voltage DC-DC boost converter," in *Proceedings of the 2015 IEEE 24th International Symposium on Industrial Electronics (ISIE)*, pp. 214–220, IEEE, Buzios, Brazil, June 2015.

[31] J. C. Kim, J. H. Huh, and J. S. Ko, "Optimization design and test bed of fuzzy control rule base for PV system MPPT in micro grid," *Sustainability*, vol. 12, no. 9, p. 3763, 2020.

[32] P. Asha, L. Natrayan, B. T. Geetha, J. R. Beulah, R. Sumathy, G. Varalakshmi, S. Neelakandan, IoT enabled environmental toxicology for air pollution monitoring using AI techniques," *Environmental Research*, vol. 205, Article ID 112574, 2022.

[33] S. Magesh, V. R. Niveditha, P. S. Rajakumar, and L Natrayan, "Pervasive computing in the context of COVID-19 prediction with AI-based algorithms," *International Journal of Pervasive Computing and Communications*, vol. 16, no. 5, pp. 477–487, 2020.

[34] K. R. Vaishali, S. R. Rammohan, L. Natrayan, D. Usha, and V. R. Niveditha, "Guided container selection for data streaming through neural learning in cloud," *International Journal of System Assurance Engineering and Management*, vol. 16, pp. 1–7, 2021.

[35] C. S. S. Anupama, L. Natrayan, E. Laxmi Lydia et al., "Deep learning with backtracking search optimization-based skin lesion diagnosis model," *Computers, Materials & Continua*, vol. 70, no. 1, pp. 1297–1313, 2021.

[36] D. K. Jain, S. K. S. Tyagi, S. Neelakandan, M. Prakash, and L. Natrayan, "Metaheuristic optimization-based resource allocation technique for cybertwin-driven 6G on IoE environment," *IEEE Transactions on Industrial Informatics*, vol. 18, no. 7, pp. 4884–4892, 2021.

[37] J. Lee, J. Jo, and H. Cha, "MPPT performance comparison between duty-cycle control and current control for photovoltaic power conditioning system," in *Proceedings of the 2018 21st International Conference on Electrical Machines and Systems (ICEMS)*, pp. 1036–1040, Jeju, Korea (South), October 2018.